



NRL/MR/6795--16-9698

Relativistic Photoionization Computations with the Time Dependent Dirac Equation

DANIEL F. GORDON
BAHMAN HAFIZI

*Beam Physics Branch
Plasma Physics Division*

October 12, 2016

Approved for public release; distribution is unlimited.

REPORT DOCUMENTATION PAGE				Form Approved OMB No. 0704-0188	
Public reporting burden for this collection of information is estimated to average 1 hour per response, including the time for reviewing instructions, searching existing data sources, gathering and maintaining the data needed, and completing and reviewing this collection of information. Send comments regarding this burden estimate or any other aspect of this collection of information, including suggestions for reducing this burden to Department of Defense, Washington Headquarters Services, Directorate for Information Operations and Reports (0704-0188), 1215 Jefferson Davis Highway, Suite 1204, Arlington, VA 22202-4302. Respondents should be aware that notwithstanding any other provision of law, no person shall be subject to any penalty for failing to comply with a collection of information if it does not display a currently valid OMB control number. <i>PLEASE DO NOT RETURN YOUR FORM TO THE ABOVE ADDRESS.</i>					
1. REPORT DATE (DD-MM-YYYY) 12-10-2016		2. REPORT TYPE Interim		3. DATES COVERED (From - To) April 2016 – August 2016	
4. TITLE AND SUBTITLE Relativistic Photoionization Computations with the Time Dependent Dirac Equation				5a. CONTRACT NUMBER	
				5b. GRANT NUMBER	
				5c. PROGRAM ELEMENT NUMBER	
6. AUTHOR(S) Daniel F. Gordon and Bahman Hafizi				5d. PROJECT NUMBER 67-4987-06	
				5e. TASK NUMBER	
				5f. WORK UNIT NUMBER	
7. PERFORMING ORGANIZATION NAME(S) AND ADDRESS(ES) Naval Research Laboratory 4555 Overlook Avenue, SW Washington, DC 20375-5320				8. PERFORMING ORGANIZATION REPORT NUMBER NRL/MR/6795--16-9698	
9. SPONSORING / MONITORING AGENCY NAME(S) AND ADDRESS(ES) Naval Research Laboratory 4555 Overlook Avenue, SW Washington, DC 20375-5320				10. SPONSOR / MONITOR'S ACRONYM(S) NRL	
				11. SPONSOR / MONITOR'S REPORT NUMBER(S)	
12. DISTRIBUTION / AVAILABILITY STATEMENT Approved for public release; distribution is unlimited.					
13. SUPPLEMENTARY NOTES					
14. ABSTRACT Ionization of inner shell electrons by laser fields often occurs in the relativistic regime. A complete description of this phenomenon requires both relativistic and quantum mechanical treatment. The Dirac equation describes the motion of a spin one-half particle in an external electromagnetic field. The stationary states in both Coulomb and soft-core potentials are solved either analytically or numerically. These are used as initial conditions in time dependent calculations. It is found that, at least in one case, two-dimensional simulations predict a greater ionization rate than the one predicted by the Coulomb corrected strong field approximation. Computational performance is important due to the rapid oscillations in a relativistic wavefunction. Multiple General Purpose Graphical Processing Units are utilized in parallel to speed up calculations.					
15. SUBJECT TERMS Tunneling Relativistic High performance computing Photoionization Dirac					
16. SECURITY CLASSIFICATION OF:			17. LIMITATION OF ABSTRACT Unclassified Unlimited	18. NUMBER OF PAGES 22	19a. NAME OF RESPONSIBLE PERSON Daniel Gordon
a. REPORT Unclassified Unlimited	b. ABSTRACT Unclassified Unlimited	c. THIS PAGE Unclassified Unlimited			19b. TELEPHONE NUMBER (include area code) (202) 767-5036

Contents

I. Introduction	1
II. Cylindrical Bound States	1
A. Starting Equations	1
B. Spin and Angular Momentum	2
C. Analytical Solutions for Coulomb Potentials	3
D. Numerical Solutions for Soft Core Potentials	6
E. Zeeman Effect	7
III. Time Dependent Simulations	8
A. Numerical Integration Technique	8
B. Validation Against Zeeman Effect	11
C. Relativistic Ionization Example	12
IV. Computational Performance	15
V. Conclusions	18
VI. Acknowledgements	18
References	19

I. INTRODUCTION

In a previous memorandum report [1] numerical solutions of the Klein-Gordon equation were developed with a view toward solution of relativistic photoionization, or other relativistic quantum electronics problems. While the Klein-Gordon equation captures much of the relevant physics, especially for moderately heavy ions ($Z \ll 137$), it does neglect the spin polarization of the electron. This memo parallels [1], but replaces the Klein-Gordon equation with the Dirac equation, which is the fully relativistic wave equation for spin one-half.

The notational and representational conventions used herein follow those of Ref. [2].

II. CYLINDRICAL BOUND STATES

A. Starting Equations

As in Ref. [1], cylindrical atoms are of interest as a reduced model that is sometimes the only one that is computationally tractable. The starting point is the symmetrical form of the Dirac equation

$$[\gamma^\mu (\hat{p}_\mu - qA_\mu) - m] \psi = 0 \quad (1)$$

where γ^μ are the contravariant Dirac matrices, \hat{p}_μ is the covariant operator of four-momentum, A_μ is the covariant four-potential, q is the charge of the particle, and m is the mass. In two dimensions this expands to

$$(i\gamma^0\partial_0 + i\gamma^1\partial_1 + i\gamma^2\partial_2 - q\gamma^0A^0 + q\gamma^1A^1 + q\gamma^2A^2 - m) \psi = 0 \quad (2)$$

Here it must be remembered superscripts are contravariant vector indices. We seek stationary states in the form

$$\psi = e^{i(\hat{\ell}\varphi - \omega x^0)} \hat{\psi} \quad (3)$$

where $\varphi = \tan^{-1}(x^2/x^1)$, and $\hat{\ell}$ is a diagonal 4×4 matrix with integer entries. Specializing further to the case of a uniform magnetic field $\mathbf{A} = \frac{1}{2}\rho B_0 \mathbf{e}_\varphi$ gives the time independent equation

$$\left(\gamma^0\omega - \gamma^0qA^0 - m + \frac{e^{i\varphi}}{2}\Gamma_+\hat{R}_+ + \frac{e^{-i\varphi}}{2}\Gamma_-\hat{R}_- \right) e^{i\hat{\ell}\varphi} \hat{\psi} = 0 \quad (4)$$

where

$$\hat{R}_\pm = \partial_\rho \pm \frac{qB_0\rho}{2} \mp \frac{\hat{\ell}}{\rho} \quad (5)$$

$$\Gamma_{\pm} = i\gamma^1 \pm \gamma^2 \quad (6)$$

Here, $\rho^2 = x^2 + y^2$. At this point it is convenient to choose a representation. We will use the standard representation in which

$$\gamma^0 = \begin{pmatrix} 1 & 0 \\ 0 & -1 \end{pmatrix} \quad \gamma^i = \begin{pmatrix} 0 & \tau_i \\ -\tau_i & 0 \end{pmatrix} \quad (7)$$

where $i \in \{1, 2, 3\}$ and τ_i are the Pauli matrices. Taking advantage of the fact that diagonal matrices commute, it is easy to show that all the terms dependent on φ cancel if and only if $\ell_1 - \ell_2 = \ell_3 - \ell_0 = 1$. If these conditions are satisfied, then

$$\left(\gamma^0 \omega - \gamma^0 q A^0 - m + \frac{1}{2} \Gamma_+ \hat{R}_+ + \frac{1}{2} \Gamma_- \hat{R}_- \right) \hat{\psi} = 0 \quad (8)$$

This is the eigenvalue equation describing the radial part of the wavefunction. It decouples into two independent systems, one for ψ^0 and ψ^3 (the spin-up solution) and one for ψ^1 and ψ^2 (the spin-down solution).

B. Spin and Angular Momentum

Due to the symmetry of the cylindrical atom, the spin-up and spin-down solutions are easily transformed into one another. Multiply the fundamental two-dimensional time dependent equation (2) on the left by $\gamma^1 \gamma^3$. Use $\{\gamma^\mu, \gamma^\nu\}_+ = 2g^{\mu\nu}$ to move $\gamma^1 \gamma^3$ to the right of the operator in parenthesis. Make a change of variables from x^1 to $\xi^1 = -x^1$. Gather the factors on the right as a new wavefunction

$$\psi'(x^0, \xi^1, x^2) = \gamma^1 \gamma^3 \psi(x^0, -\xi^1, x^2) \quad (9)$$

If the components of A^μ all have definite parity with respect to x^1 , ψ' satisfies the original equation, with possible changes in the signs of A^μ . For A^0 and A^2 , odd parity results in a sign change. For A^1 , even parity results in a sign change.

Now consider a cylindrical Dirac atom in a constant magnetic field. The field configuration has A^0 even, A^1 even, and A^2 odd. Thus the scalar potential of the transformed problem is unchanged, but the magnetic field is reversed. The sign of φ is also reversed, due to the coordinate reversal, but this is more conveniently viewed as a transformation of $\hat{\ell}$.

Specifically, if there is a stationary state $\psi(x^0, \rho, \varphi; -B_0, \hat{\ell})$, then there is also a stationary state

$$\psi'(x^0, \rho, \varphi; B_0, \hat{\ell}') = e^{i(\ell'\varphi - \omega x^0)} \begin{pmatrix} \hat{\psi}^1(\rho; -B_0) \\ -\hat{\psi}^0(\rho; -B_0) \\ \hat{\psi}^3(\rho; -B_0) \\ -\hat{\psi}^2(\rho; -B_0) \end{pmatrix} \quad (10)$$

where $\ell'_0 = -\ell_1$, $\ell'_1 = -\ell_0$, $\ell'_2 = -\ell_3$, and $\ell'_3 = -\ell_2$. Note that a spin-up solution is transformed into a spin-down solution and vice-versa.

It is instructive to consider the angular momentum of the system. The operator of total angular momentum is

$$\hat{j}_z = \frac{1}{2}\Sigma_z - i\partial_\varphi \quad (11)$$

where the first term is due to the spin (see Ref. [2]). The eigenvalues are $j_z = \ell_0 + \frac{1}{2}$ in the case of a spin-up state, or $j_z = \ell_1 - \frac{1}{2}$ for a spin-down state. If the transformation (10) is applied, the sign of j_z is reversed. The total angular momentum is a good quantum number. The orbital angular momentum is a bad quantum number because the stationary states have $\ell_0 \neq \ell_3$ and $\ell_1 \neq \ell_2$, so that they are not eigenfunctions of ∂_φ . Any spin-up bound state is fully specified by a radial quantum number, n_r (see below), and the total angular momentum j_z . In the following we treat only the spin-up state, since the spin-down state can always be obtained by the transformation (10). A specific spin-up state is denoted by the ket $|n_r, j_z\rangle$

C. Analytical Solutions for Coulomb Potentials

In the case of a Coulomb potential, $A^0 = Q/\rho$, where Q is the effective nuclear charge [11], it is possible to obtain an analytical solution in the limit of a weak magnetic field. Define Q_1 and Q_2 such that $\psi_0 = \sqrt{m + \omega}\rho^s e^{-\lambda\rho}(Q_1 + Q_2)$ and $\psi_3 = i\sqrt{m - \omega}\rho^s e^{-\lambda\rho}(Q_1 - Q_2)$, where $\lambda = \sqrt{m^2 - \omega^2}$ and $s = -1/2 + \sqrt{j_z^2 - q^2 Q^2}$. Then one obtains the following uncoupled equations for Q_1 and Q_2 :

$$\begin{aligned} & \rho Q_1'' + \left(1 + 2\sigma - 2\lambda\rho + \frac{m\omega_c\rho^2}{j_z - Z_m - \frac{m\omega_c\rho^2}{2}}\right) Q_1' + \\ & \left[j_z m\omega_c\rho - \frac{m^2\omega_c^2\rho^3}{4} + \left(\frac{m\omega_c\rho}{j_z - Z_m - \frac{m\omega_c\rho^2}{2}} - 2\lambda\right)(\sigma + Z_\omega)\right] Q_1 = 0 \end{aligned}$$

$$\rho Q_2'' + \left(1 + 2\sigma - 2\lambda\rho + \frac{m\omega_c\rho^2}{j_z - Z_m - \frac{m\omega_c\rho^2}{2}}\right) Q_2' + \left[j_z m\omega_c\rho - \frac{m^2\omega_c^2\rho^3}{4} + \frac{m\omega_c\rho(\sigma - Z_\omega)}{j_z + Z_m - \frac{m\omega_c\rho^2}{2}} - 2\lambda\left(1 + \sigma + Z_\omega + \frac{m\omega_c\rho^2}{j_z + Z_m - \frac{m\omega_c\rho^2}{2}}\right)\right] Q_2 = 0$$

where $Z_m = qQm/\lambda$, $Z_\omega = qQ\omega/\lambda$, $\sigma = s + 1/2$, and $\omega_c = qB_0/m$. In the low field limit $|m\omega_c|\rho^2 \ll 4|j_z|$ and $|m\omega_c|\rho^2 \ll 2|j_z \pm Z_m|$ assuming ρ is bounded. Supposing further that $|\sigma \pm Z_\omega|/|j_z \mp Z_m| \ll j_z$ results in

$$Q_1'' + \left(\frac{1+2\sigma}{\rho} - 2\lambda\right) Q_1' + \left[m\omega_c j_z - \frac{2\lambda}{\rho}(\sigma + Z_\omega)\right] Q_1 \approx 0 \quad (12)$$

$$Q_2'' + \left(\frac{1+2\sigma}{\rho} - 2\lambda\right) Q_2' + \left[m\omega_c j_z - \frac{2\lambda}{\rho}(1 + \sigma + Z_\omega)\right] Q_2 \approx 0 \quad (13)$$

The solutions that are finite for $\rho = 0$ are

$$Q_1 = C_1 e^{(\lambda-\beta)\rho} F\left[\frac{(-1 + 2Z_\omega)\lambda + (1 + 2\sigma)\beta}{2\beta}, 1 + 2\sigma, 2\beta\rho\right] \quad (14)$$

$$Q_2 = C_2 e^{(\lambda-\beta)\rho} F\left[\frac{(1 + 2Z_\omega)\lambda + (1 + 2\sigma)\beta}{2\beta}, 1 + 2\sigma, 2\beta\rho\right] \quad (15)$$

$$\frac{C_1}{C_2} = \frac{\sigma - Z_\omega}{j_z + Z_m} \quad (16)$$

where $F(a, b, z)$ is the confluent hypergeometric function [12] and $\beta = \sqrt{\lambda^2 - m\omega_c j_z}$. The energy levels for the bound states are found by demanding that the wavefunction should vanish as $\rho \rightarrow \infty$. Then the first argument of F must be a negative integer or zero. Thus, the energy eigenvalues for a weak field B_0 , total angular momentum j_z , and radial quantum number n_r are determined from

$$\frac{(\mp 1 + 2Z_\omega)\lambda + (1 + 2\sigma)\beta}{2\beta} = -n_r \quad (17)$$

where $n_r \in \{0, 1, 2, \dots\}$. An important point to note is that for $B_0 \neq 0$, it is not always possible to satisfy both equations simultaneously (see discussion of Zeeman splitting below). The validity of the assumptions used to obtain (17) cannot be decoupled from the particular state considered. Sufficiently far from the axis ($\rho \rightarrow \infty$), the approximations involving the smallness of $|m\omega_c|\rho^2$ will always break down. It is expected, therefore, that states whose

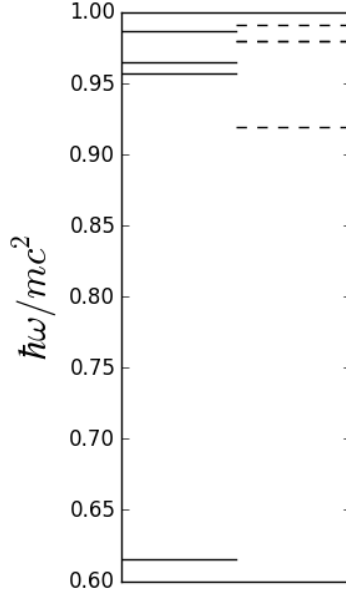


FIG. 1: First few energy levels of cylindrical (solid) and spherical (dashed) hydrogen-like xenon according to Dirac theory with $B_0 = 0$.

wavefunction decays rapidly with ρ are approximated best. These are generally the states with the lowest energy.

In the case where $B_0 = 0$ the energy eigenvalues can be expressed as

$$\omega = m \left[1 + \frac{q^2 Q^2}{\left(n_r + \sqrt{j_z^2 - q^2 Q^2} \right)^2} \right]^{-1/2} \quad (18)$$

Because of the square root, the cylindrical Dirac ion (with perfect Coulomb potential) can only be in an s -state provided $q^2 Q^2 < 1/4$. In terms of the atomic number, $Z = -Q/q$, assuming the orbiting charge is an electron, this condition is expressed as $Z \leq 68$. This differs from the spin zero (Klein-Gordon) case where no s -state is possible at all for a cylindrical Coulomb ion.

Fig. 1 compares the first few energy levels in a cylindrical hydrogen-like xenon ion ($Z = 54$) with those of the corresponding spherical ion. The qualitative structure of the energy levels is similar, but in cylindrical geometry each energy level is lowered relative to its spherical counterpart. The fact that the energy is lowered is fortuitous, because, as will be shown below, a soft-core potential can be used to raise the energy of the cylindrical state so that it becomes commensurate with the corresponding spherical state.

D. Numerical Solutions for Soft Core Potentials

In order to compute the stationary states of a Dirac ion in a magnetic field without any approximation, one may return to the fundamental Eq. (8) and solve it numerically. The primary difficulty is that the Coulomb potential has a singularity which is not amenable to discretization. One solution that is often employed is to use a soft-core potential

$$A^0 = \frac{Q}{\sqrt{\rho^2 + \delta\rho^2}} \quad (19)$$

where $\delta\rho$ is a constant called the soft core radius. The soft core potential converges to a Coulomb potential as $\delta\rho \rightarrow 0$. Depending on the state considered, a very small value of $\delta\rho$ might have to be used, in conjunction with a similarly small numerical cell size, in order to satisfactorily approximate the Coulomb solution.

Let each component of $\hat{\psi}(\rho)$ be discretized on a sequence of mesh points $\{\rho_i = (2i - 1)\frac{\Delta\rho}{2} | i \in \mathbb{N}\}$. Evaluating the derivatives in Eq. (8) via centered finite differences gives a $4N \times 4N$ block tridiagonal matrix equation, where N is the number of mesh points used. This breaks into two independent $2N \times 2N$ systems, one for spin up, the other for spin down. The spin up part is

$$\begin{pmatrix} D_+ & -iT_- \\ -iT_+ & D_- \end{pmatrix} \begin{pmatrix} \hat{\psi}^0 \\ \hat{\psi}^3 \end{pmatrix} = \omega \begin{pmatrix} \hat{\psi}^0 \\ \hat{\psi}^3 \end{pmatrix} \quad (20)$$

where T_{\pm} are tridiagonal, and D_{\pm} are diagonal. The non-zero elements of T_{\pm} and D_{\pm} are

$$T_{\pm,i,i-1} = -\frac{1}{2\Delta\rho} \quad (21a)$$

$$T_{\pm,i,i} = \frac{1/2 \mp j_z}{\rho_i} \pm \frac{qB_0\rho_i}{2} \quad (21b)$$

$$T_{\pm,i,i+1} = \frac{1}{2\Delta\rho} \quad (21c)$$

$$D_{\pm,i,i} = qA_i^0 \pm m \quad (21d)$$

where $A_i^0 = A^0(\rho_i)$. The spin down part is obtained from the same system with the signs of j_z and B_0 reversed, and the column vector replaced by $(\hat{\psi}^1, \hat{\psi}^2)$. The spin down solutions obtained from the transformation (10) are identical, as exemplified in Fig. 2. Standard sparse

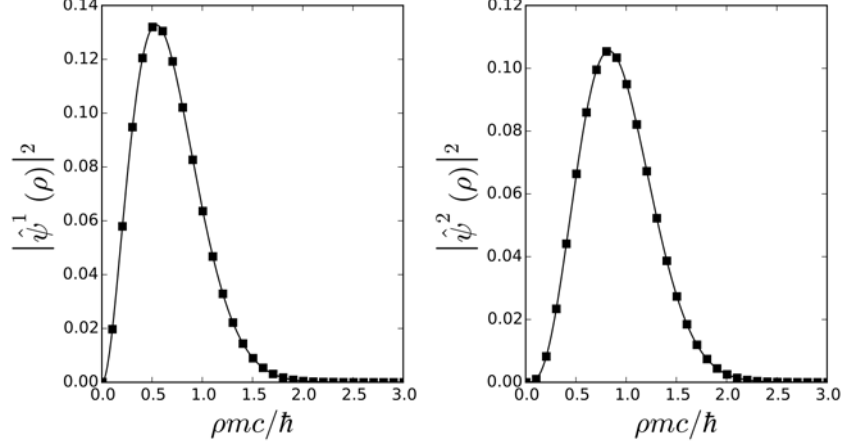


FIG. 2: Spin down wavefunction computed directly (solid lines), and using the transformation (10) (squares). The parameters of the numerical atom are $Z = 54$, $\Delta\rho = 0.01$, $\delta\rho = 0.1$, $j_z = 1/2$, and $n_r = 0$. The magnetic field is $\hbar\omega_c/mc^2 = 3.4$.

matrix packages can solve the eigensystem for various subsets of the eigenvalue-eigenvector pairs. A similar system can be constructed for spherical atoms.

An important question is how small the soft-core radius must be in order to achieve a given error tolerance with respect to the ideal Coulomb solution. The ideal Coulomb solution is known exactly in the case where $B_0 = 0$. Fig. 3 shows the convergence of the numerical solution to the Coulomb solution for the lowest three bound states of cylindrical hydrogen-like xenon ($Z = 54$). The cell size and the soft-core radius are set equal in all cases. Not surprisingly, the $|0, \frac{1}{2}\rangle$ state is the hardest to resolve, requiring $\delta\rho = 10^{-4}$ to reduce the error to less than 1%. For comparison, the characteristic size of the $|0, \frac{1}{2}\rangle$ state for $Z = 54$ is $1/\lambda \approx 1.2$.

E. Zeeman Effect

In the case of the Klein-Gordon equation for spin zero it is possible to obtain an analytical description of the Zeeman effect, to first order in the magnetic field. In the case of spin $1/2$, the situation is more complicated. As noted above, the approximations used to obtain Eq. (17) are subtly dependent on the particular state considered. Moreover, in a magnetic field, there may be no choice of radial quantum number that simultaneously forces both hypergeometric functions in the solution to zero as $\rho \rightarrow \infty$. This situation is alluded to

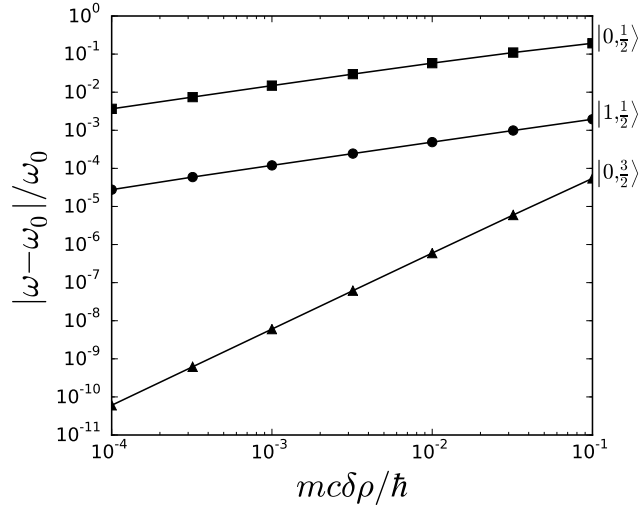


FIG. 3: Convergence of the three lowest cylindrical bound state energies of hydrogen-like xenon with diminishing soft core radius, $\delta\rho$. The energy in a perfect Coulomb potential is denoted ω_0 .

in Refs. [3, 4]. On the other hand, we are always able to find well behaved numerical solutions in a soft-core potential. One explanation for this is that the requirement that both hypergeometric functions vanish as $\rho \rightarrow \infty$ is a sufficient, but not necessary condition, on the normalizability of the wavefunction.

Based on the information in Fig. 3, one can check the accuracy of Eq. (17) against the numerical soft-core solution, given a sufficiently small soft-core radius. Fig. 4 shows such a comparison for the $|0, \pm\frac{1}{2}\rangle$ state with $\delta\rho = 10^{-5}$ and for the $|1, \pm\frac{1}{2}\rangle$ and $|0, \pm\frac{3}{2}\rangle$ states with $\delta\rho = 10^{-3}$. The approximations used in the analytical formula work surprisingly well except for the $|1, \frac{1}{2}\rangle$ state.

III. TIME DEPENDENT SIMULATIONS

A. Numerical Integration Technique

In the standard representation of the symmetrical form of the Dirac equation, the “electron” components (ψ^0 and ψ^1) depend only on spatial derivatives of the “positron” components (ψ^2 and ψ^3), and vice-versa. This suggests an efficient time integration scheme where the electron and positron components are leap-frogged over each other. To see how this works, it is convenient to put the Dirac equation in the Hamiltonian form $i\partial_0\psi = H\psi$ (this

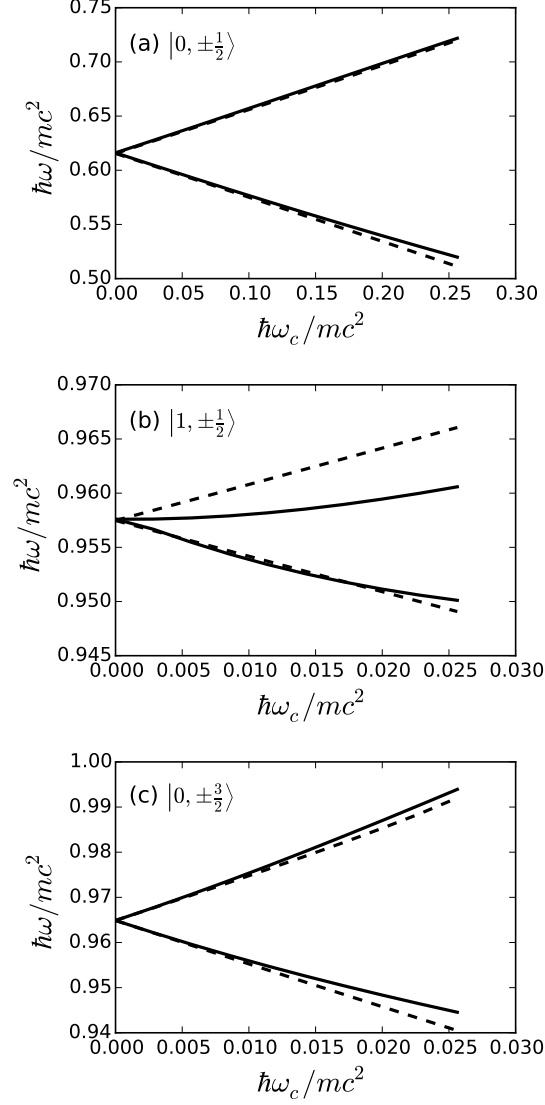


FIG. 4: Weak field (dashed) and numerical (solid) solution for energy levels in cylindrical hydrogen-like xenon for the states (a) $|0, \pm\frac{1}{2}\rangle$, (b) $|1, \pm\frac{1}{2}\rangle$, and (c) $|0, \pm\frac{3}{2}\rangle$. The upper branches are for positive j_z and the lower branches are for negative j_z . For reference, $\hbar\omega_c/mc^2 = 1$ corresponds to a magnetic field of 44 TG.

in no way scrambles the components of the wavefunction). The Hamiltonian is conveniently expressed in 2×2 block form as

$$H = \begin{pmatrix} D_+ & S \\ S & D_- \end{pmatrix} \quad (22)$$

where

$$D_{\pm} = qA^0 \pm m \quad (23)$$

$$S = \begin{pmatrix} -i\partial_3 & -i\partial_1 - \partial_2 \\ -i\partial_1 + \partial_2 & i\partial_3 \end{pmatrix} + q \begin{pmatrix} -A^3 & -A^1 + iA^2 \\ -A^1 - iA^2 & A^3 \end{pmatrix} \quad (24)$$

In order to express the leapfrog scheme in a compact and transparent way, the Hamiltonian is expressed as $H = H^{(11)} + H^{(12)} + H^{(21)} + H^{(22)}$, where

$$H^{(11)} = \begin{pmatrix} D_+ & 0 \\ 0 & 0 \end{pmatrix} \quad H^{(12)} = \begin{pmatrix} 0 & S \\ 0 & 0 \end{pmatrix} \quad (25)$$

$$H^{(21)} = \begin{pmatrix} 0 & 0 \\ S & 0 \end{pmatrix} \quad H^{(22)} = \begin{pmatrix} 0 & 0 \\ 0 & D_- \end{pmatrix} \quad (26)$$

Define $\phi = (\psi^0, \psi^1)$ and $\chi = (\psi^2, \psi^3)$. Suppose ϕ is known at time level $n - 1/2$, while χ is known at time level n . The wavefunction is advanced in two steps using

$$\psi(t + \Delta t/2) = e^{-iH^{(12)}\Delta t/2} e^{-iH^{(11)}\Delta t} e^{-iH^{(12)}\Delta t/2} \psi(t) \quad (27)$$

$$\psi(t + \Delta t) = e^{-iH^{(21)}\Delta t/2} e^{-iH^{(22)}\Delta t} e^{-iH^{(21)}\Delta t/2} \psi(t + \Delta t/2) \quad (28)$$

Here, $\psi(t + T)$ must be interpreted with care. If $T/\Delta t$ is a half integer, the argument gives the time at which ϕ is known, with χ being known a half-step earlier. If $T/\Delta t$ is an integer, the argument gives the time at which χ is known, with ϕ being known a half-step earlier.

The integration scheme of Eqs. (27) and (28) amounts to a carefully chosen factorization of the operator exponential, $e^{-iH\Delta t}$. Leapfrogging ϕ and χ corresponds to factorizing the upper and lower rows. Each step in the leapfrog scheme is further factorized. In particular, the off-diagonal elements are split, and arranged so that the two halves bracket the diagonal element. This can be shown to eliminate the lowest order factorization error that would occur if the off-diagonal elements were kept together.

The formal expressions (27) and (28) have to be further approximated to be useful computationally. In this work the factors corresponding to the off-diagonal part of the Hamiltonian are replaced by the lowest order Taylor expansion. This gives the explicit formulas

$$\phi(t + \Delta t/2) = \exp(-iD_+\Delta t) \left[\phi(t - \Delta t/2) - iS\chi(t) \frac{\Delta t}{2} \right] - iS\chi(t) \frac{\Delta t}{2} \quad (29)$$

$$\chi(t + \Delta t) = \exp(-iD_-\Delta t) \left[\chi(t) - iS\phi(t + \Delta t/2) \frac{\Delta t}{2} \right] - iS\phi(t + \Delta t/2) \frac{\Delta t}{2} \quad (30)$$

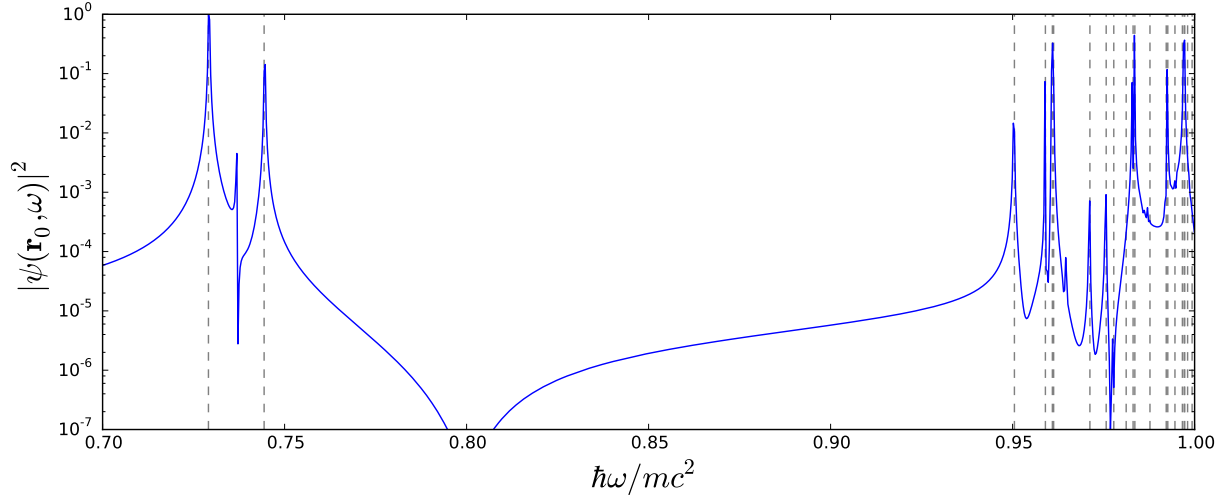


FIG. 5: Comparison of energy levels in a cylindrical soft core potential with $Z = 54$ and $B_0 = 0.2$, as determined by time dependent (solid) and time independent (dashed) calculations. The broad features in the time dependent result are only visible on a log scale.

This requires only explicit finite difference evaluations and two special function evaluations. Note that the diagonal part of the Hamiltonian is treated such that unitarity is preserved to machine precision. The entire scheme turns out to preserve unitarity to several digits of precision, as is demonstrated below.

B. Validation Against Zeeman Effect

A general method for determining the energy levels of a numerical atom using a time dependent code was given in Ref. [1]. The method is used here to test the algorithm for integrating the time dependent Dirac equation given above. The energy levels falling out of the time dependent calculation have to be generated for a soft-core potential, and so are most conveniently compared with the numerical time independent calculation. This comparison validates the time dependent calculation provided the time independent calculation itself is validated. This latter validation has already been provided in the form of comparisons with analytical energy levels in a Coulomb potential and constant magnetic field.

In carrying out the time dependent calculation, a random wavefunction is initialized in a soft core potential with $Z = 54$ and $\delta\rho = 0.1$. The number of grid cells is 2000×2000 , the number of time steps is 2^{20} , the cell size is 0.05×0.05 , and the time step is 0.02. The

most important parameter for this purpose is the number of steps, which needs to be large in order to resolve narrowly separated spectral lines. As can be seen in Fig. 5, the peaks of the time dependent spectrum neatly line up with the dashed lines, which denote the discrete energies predicted by the time independent calculation. The vertical axis spans several orders of magnitude so that the effects of a finite temporal window can be seen. The relative strength of each spectral line is a function of the point in space, \mathbf{r}_0 , where the time dependence of the wavefunction is analyzed. In fact, if \mathbf{r}_0 happens to be near a null of a particular eigenfunction, the associated energy eigenvalue may not appear in the numerical spectrum. In Fig. 5, the diagnostic point is $\mathbf{r}_0 = \mathbf{e}_1 + \mathbf{e}_2$, where \mathbf{e}_i are Cartesian basis vectors.

C. Relativistic Ionization Example

One important application of numerical solution of the time dependent Dirac equation is in modeling relativistic photoionization processes. In Ref. [1] an example is given using the spin zero Klein-Gordon equation. In the Klein-Gordon case, the parameters of the ionization problem are the radiation frequency, ω_0 , the peak vector potential, A_0 , and the atomic number of the hydrogen-like ion, Z . In the case of the Dirac equation, an additional parameter must be considered: the orientation of the electron spin with respect to the radiation polarization and wavevector. In the two-dimensional geometry considered in this report, it is only possible to consider the case where the radiation polarization is orthogonal to the spin. The form of the vector potential is

$$\mathbf{A}(\mathbf{r}, t) = A_0 [\cos(\mathbf{k} \cdot \mathbf{r} - \omega_0 t) - 1] \Theta(\omega_0 t - \mathbf{k} \cdot \mathbf{r}) \mathbf{e}_R \quad (31)$$

where Θ is the Heaviside step function, and $\mathbf{k} \cdot \mathbf{e}_R = 0$. In three dimensions, nothing constrains the choice of \mathbf{e}_R relative to the spin. In two dimensions, \mathbf{e}_R cannot have a component in the ignorable direction, for otherwise a momentum would be induced in that direction, leading to a contradiction. Hence, if the spin is chosen to be in the ignorable direction, the radiation and electron polarizations must be orthogonal. In this report, $\mathbf{k} \parallel \mathbf{e}_1$, $\mathbf{e}_R = \mathbf{e}_2$, and the spin is aligned with \mathbf{e}_3 . The electrostatic potential is a soft core potential, with $\delta\rho$ chosen so that the ground state energy of the cylindrical ion coincides with the ground state energy of the Coulombic spherical ion with the same Z . The product $\omega_0 A_0$ is chosen so that the corresponding electric field coincides with the barrier suppression

Parameter	Symbol	Value
Initial State	$ n_r, j_z\rangle$	$ 0, \frac{1}{2}\rangle$
Steps	N_t	2^{16}
Cells	$N_x \times N_y$	$2^{14} \times 2^{14}$
Time Step	Δt	$0.03\hbar/mc^2$
Space Step	$\Delta x, \Delta y$ or $\Delta x, \Delta z$	$0.12\hbar/mc$
Residual Charge	Z	54
Soft Core Radius	$\delta\rho$	$1.9\hbar/mc$
Laser wavelength	λ	1.52 nm
Vector Potential	A_0	$2.6mc^2/e$

TABLE I: Parameters for simulation of relativistic ionization

threshold model [5]. There is a constraint imposed by limited computation time, which tends to increase ω_0 . For the example given here, ω_0 is chosen to make the simulation time a few hours on a 16-GPGPU cluster, while keeping the adiabaticity parameter in the tunneling regime. The simulation parameters are given in Table I. The initial bound state is computed by solving (8) and resampling the result on the Cartesian grid of the time dependent problem.

The simulated ionization rate is defined in terms of the charge current flowing out of a volume containing the bound state. Solutions of the Dirac equation satisfy the continuity equation $\partial_\mu j^\mu = 0$ where $j^\mu = q\psi^\dagger \gamma^0 \gamma^\mu \psi$. In three dimensional form, $\partial_t \varrho + \nabla \cdot \mathbf{j} = 0$, where

$$\varrho = q\psi^\dagger \psi \quad (32)$$

The expectation value of the charge contained in a ball \mathcal{B} is

$$\langle q \rangle_{\mathcal{B}} = \int_{\mathcal{B}} d^3\mathbf{r} \varrho \quad (33)$$

Take the radius of \mathcal{B} to be large enough so that it contains the charge associated with the bound state almost entirely. Then the ionization probability is defined as the expectation value of the charge outside \mathcal{B} , divided by the total charge of the particle:

$$\mathcal{P} = \frac{q - \langle q \rangle_{\mathcal{B}}}{q} \quad (34)$$

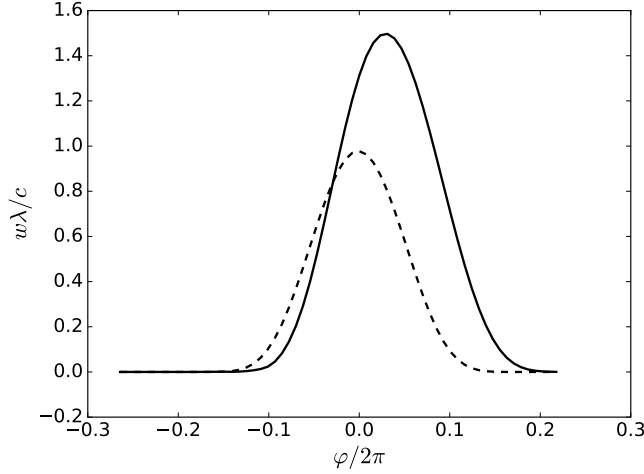


FIG. 6: Simulated and analytical ionization rates. The solid curve is the simulated rate, defined as in (35), where \mathcal{B} is a cylinder of radius 20λ . The dashed curve is based on the dressed Coulomb corrected S -matrix analysis of Ref. [6]. In plotting the dashed curve a factor was inserted to unwind cycle averaging.

The ionization rate is

$$W = \frac{d\mathcal{P}}{dt} = -\frac{1}{q} \frac{\partial}{\partial t} \int_{\mathcal{B}} d^3\mathbf{r} \varrho \quad (35)$$

which by the divergence theorem, is the same as the current flowing out of the volume, divided by the charge.

It is of interest to compare the simulated ionization rate with various analytical formulas. In this report we make comparison with the dressed Coulomb corrected S -matrix theory of Ref. [6]. Strictly, the S -matrix theory gives the ionization rate averaged over an optical period. However, in the adiabatic limit, the cycle averaging can be unwound, and the rate can be considered an instantaneous function of the field [7–10]. The result of this procedure is shown in Fig. 6. The simulated rate is larger than that of the S -matrix prediction. The peak simulated rate is delayed with respect to the peak of the electric field ($\varphi = 0$) because of the propagation delay between the ionic core and the diagnostic sphere $\partial\mathcal{B}$.

A useful measure of the accuracy of any simulation of photoionization is the precision with which charge is conserved. Fig. 7 shows the evolution of the charge error, normalized to the electronic charge, during the course of the simulation. The accuracy is about 6 digits until significant ionization sets in. The accuracy drops to about 4 digits by the end of the simulation.

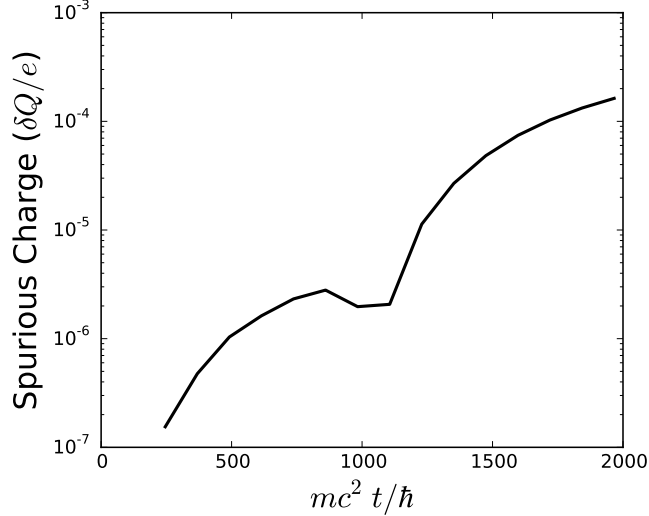


FIG. 7: Accuracy of charge conservation during the course of the simulation of relativistic tunneling ionization. The error in the total charge is denoted δQ .

Finally, a visualization of the ionizing wavefunction is shown in Fig. 8. The electric field points in the $-y$ -direction and the radiation wavevector points in the x -direction. As expected, the ionized wavepacket is extracted opposite the direction of the electric field, and is also pushed in the direction of the radiation momentum.

IV. COMPUTATIONAL PERFORMANCE

The programming model used for the Dirac equation follows, almost without modification, the methods given in Ref. [1] for the Klein-Gordon equation. The primary difference is that in the case of the Dirac equation, additional synchronization is necessary to guarantee that the electron state, ϕ , is updated before advancing the positron state, χ . The simplest way to do this is to use two separate OpenCL kernels to advance ϕ and χ . Apart from this distinction, all the methods for distributing the workload on a cluster of GPGPUs remain the same.

The floating point precision used in the code can be selected at compile time. Single precision is suitable for cases where one is interested in a final state which is significantly different from the initial state. If the initial state is weakly perturbed, accuracy typically demands that double precision to be used.

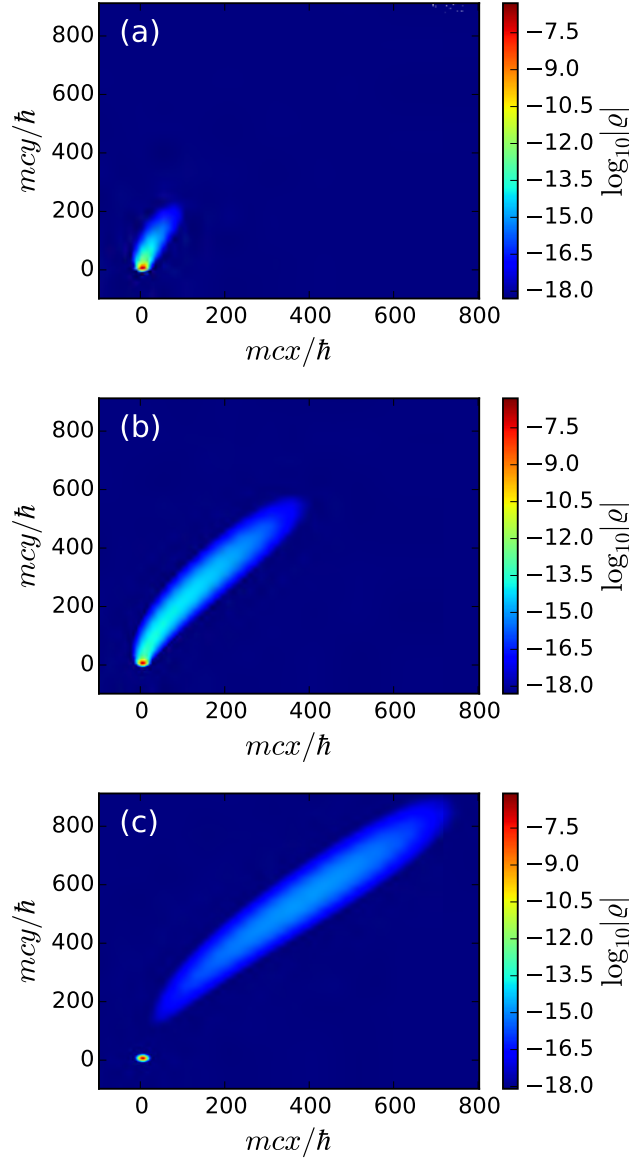


FIG. 8: Charge density associated with ionizing relativistic wavefunction evaluated at (a) $mc^2t/\hbar = 490$, (b) $mc^2t/\hbar = 980$, and (c) $mc^2t/\hbar = 1470$.

The performance on various GPGPU devices is given in Fig. 9, for single and double precision, using a 2000×2000 numerical grid. The performance penalty for using double precision is about two-fold on the gaming device (NVIDIA Geforce GTX 980), and somewhat less on the other devices. The water cooled device advances about 350 million cells per second. Performance could likely be improved by optimizing memory access patterns.

The performance on a cluster of GPGPU devices, namely the SGI ICE X system “Topaz”

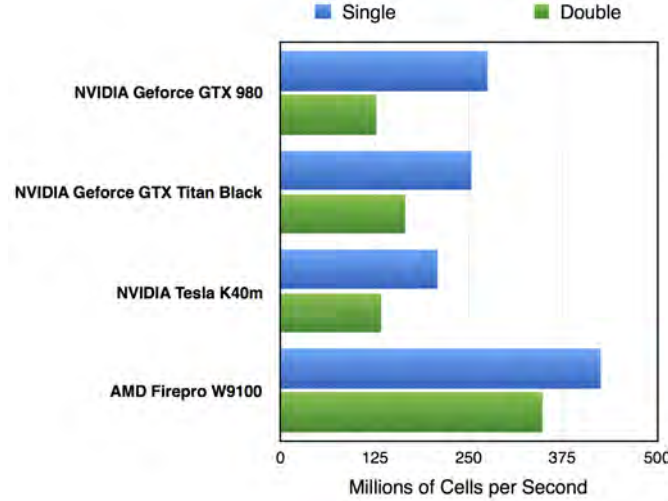


FIG. 9: Performance in terms of millions of cells per second for various GPGPUs. Blue bars are for single precision and green bars are for double precision. The Firepro W9100 is water cooled.

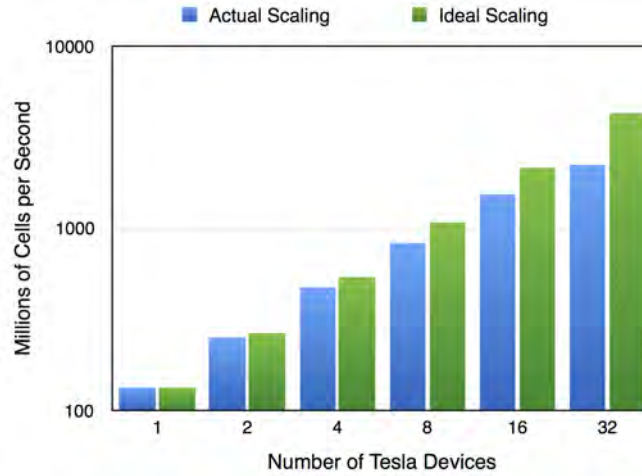


FIG. 10: Strong scaling study on the DoD HPCMP cluster “Topaz” in terms of millions of cells per second in the aggregate. Double precision is used in all cases. One GPGPU is assigned to each MPI node.

at the U.S. Army Engineer Research and Development Center (ERDC), is given in Fig. 10. The Topaz system has 32 GPU nodes, each with a single NVIDIA Tesla K40P device. Fig. 10 gives scaling results for a 2000×2000 numerical grid. In going from 16 to 32 nodes, performance is still gained, so the strong scaling limit is not reached. In order to carry out a meaningful weak scaling study, a larger GPGPU cluster would be needed.

V. CONCLUSIONS

Numerical solution of the Dirac equation is applied to the problem of relativistic tunneling ionization. Analytical and numerical solutions of the time independent equation are used to obtain the initial wavefunction as a bound state of a soft-core potential. An efficient numerical integration scheme for the time dependent equation is developed to advance the initial wavefunction in the presence of a relativistically intense electromagnetic wave. The numerical scheme is implemented to take advantage of clusters of GPGPU devices. It is found that the numerical ionization rate exceeds the dressed Coulomb corrected SFA rate.

VI. ACKNOWLEDGEMENTS

This work was supported by the NRL 6.1 base program.

-
- [1] D.F. Gordon, B. Hafizi, and M.H. Helle. Numerical relativistic quantum optics. Technical Report NRL/MR/6790–13-9496, Naval Research Laboratory, 2013.
 - [2] V.B. Berestetsky, E.M. Lifshitz, and L.P. Pitaevskii. *Quantum Electrodynamics*. Pergamon Press, 1980.
 - [3] C.-L. Ho and V.R. Khalilov. Planar Dirac electron in Coulomb and magnetic fields. *Phys. Rev. A*, 61:032104–1–032104–7, Feb 2000.
 - [4] C.-M. Chiang and C.-L. Ho. Planar Dirac electron in Coulomb and magnetic fields: A Bethe ansatz approach. *J. Mathematical Phys.*, 43:43–51, Jan 2002.
 - [5] S. Augst, D. Strickland, D.D. Meyerhofer, S.L. Chin, and J.H. Eberly. Tunneling ionization of noble gases in a high-intensity laser field. *Phys. Rev. Lett.*, 63(20):2212–2215, Nov 1989.
 - [6] M. Klaiber, E. Yakaboylu, and K.Z. Hatsagortsyan. Above-threshold ionization with highly charged ions in superstrong laser fields. II. Relativistic Coulomb-corrected strong-field approximation. *Phys. Rev. A*, 87:023418–1–023418–11, 2013.
 - [7] A.M. Perelemov, V.S. Popov, and M.V. Terent’ev. Ionization of atoms in an alternating electrical field. *Soviet Physics JETP*, 23(5):924–934, 1966.
 - [8] A.M. Perelemov, V.S. Popov, and M.V. Terent’ev. Ionization of atoms in an alternating electrical field. ii. *Soviet Physics JETP*, 24(1):207, 1967.
 - [9] A.M. Perelemov and V.S. Popov. Ionization of atoms in an alternating electrical field. iii. *Sov. Phys. JETP*, 25(2):336–343, Aug 1967.
 - [10] A.M. Perelemov, V.S. Popov, and V.P. Kuznetsov. Allowance for the Coulomb interaction in multiphoton ionization. *Soviet Physics JETP*, 27(3):451–457, 1968.
 - [11] In cylindrical geometry this form implies a distributed charge
 - [12] We adopt the nomenclature of L.D. Landau and E.M. Lifshitz, *Quantum Mechanics*, Eq. (d4). The confluent hypergeometric function is denoted by M in Abramowitz and Stegun.

